The L-H Transition and the Stability of the Edge Pedestal

B. N. Rogers, J. F. Drake
Institute for Plasma Research, University of Maryland, College Park, MD 20742, USA
A. Zeiler
Max-Planck-Institut für Plasmaphysik, EURATOM Association, 85748 Garching, Germany

November 10, 1998

Abstract

Based on three-dimensional simulations of the Braginskii equations, we identify two main parameters which control transport in the edge of tokamaks: the MHD ballooning parameter and a diamagnetic parameter. The space defined by these parameters delineates regions where typical L-mode levels of transport arise, where the transport is catastrophically large (density limit) and where the plasma spontaneously forms a transport barrier (H-mode). Ion diamagnetic effects allow the edge pedestal to steepen well beyond the first ideal MHD stability boundary.

1 Introduction

The tokamak edge region vitally controls the plasma discharge through its role in the L-H transition[1, 2], the density limit [3], and the edge temperature pedestal. We suggest here, based on three-dimensional simulations of the Braginskii equations, that these phenomena are fundamentally linked to the dependence of the turbulent edge transport on two dimensionless parameters: the MHD ballooning parameter $\alpha = -Rq^2 d\beta/dr$ and a diamagnetic parameter α_d (defined below). The space spanned by these parameters is shown in Fig. (1). In the weak diamagnetic limit (small α_d), the simulations show a dramatic rise in the transport with increasing α that leads to high transport levels even at small α values well below the limit of ideal ballooning instability[4, 5]. We associate this behavior with an effective density limit beyond which stable tokamak operation is not possible [6]. At higher $\alpha_d \sim 1$, on the other hand, the α dependence of the turbulence is reversed, with small but finite values of α leading to a strong suppression of transport. In this regime a local increase in the plasma pressure gradient, above a threshold in α, causes a *reduction* of the transport [6]. Since such a reduction would naturally lead to a further steepening of the edge pressure gradient, this region of higher α and α_d is unstable to the spontaneous formation of a transport barrier. The boundary of this unstable domain defines the onset condition for the L-H transition in our model. Finally, the global stability of the edge pedestal and the relative roles of finite α and $E \times B$ shear are explored in dynamical simulations of the barrier formation process. These simulations confirm the $E \times B$ shear effect can stabilize turbulence during the formation of the barrier [7, 8]. We also find, however, that for small α, $E \times B$ shear alone is not sufficient to trigger a transition due to the strong positive dependence of transport on the plasma pressure gradient [6].

2 Model

The simulations are based on a shifted-circle magnetic geometry and are carried out in a poloidally and radially localized, flux-tube domain that winds around the torus [9]. We evolve six nonlinear equations, summarized in Ref.[6], for the perturbations of the magnetic flux $\tilde{\psi}$, electric potential $\tilde{\phi}$, density $\tilde{n}$, electron and ion temperatures $\tilde{T}_e$, $\tilde{T}_i$, and parallel flow $\tilde{v}_{||}$. For later reference in the text, we show here only the isothermal limit of the full system ($\tilde{T}_e, \tilde{T}_i \to 0$), neglecting the (small) contributions of $\tilde{v}_{||}$ and magnetic pumping:

$$(2\pi)^2\alpha\left(\partial_t\tilde{\psi} + \alpha_d\partial_y\tilde{\psi}\right) - \nabla_{||}\left(\tilde{\phi} - \alpha_d\tilde{n}\right) = \tilde{J}, \tag{1}$$

$$\nabla_\perp \cdot D_t\nabla_\perp(\tilde{\phi} + \tau\alpha_d\tilde{n}) + \hat{C}\tilde{n} - \nabla_{||}\tilde{J} = 0, \tag{2}$$

$$D_t\tilde{n} + \partial_y\tilde{\phi} - \epsilon_n\hat{C}(\tilde{\phi} - \alpha_d\tilde{n}) - \alpha_d\epsilon_n(1+\tau)\nabla_{||}\tilde{J} = 0, \tag{3}$$

where $\nabla_{||} = \partial_z + (2\pi)^2\alpha\ \vec{z}\times\nabla_\perp\tilde{\psi}\cdot\nabla_\perp$, $D_t = \partial_t + \vec{z}\times\nabla_\perp\tilde{\phi}\cdot\nabla_\perp$, $\nabla_\perp^2 = (\partial_x + \Lambda(z)\partial_y)^2 + \partial_y^2$, $\hat{C} = (\cos(2\pi z) + \Lambda(z)\sin(2\pi z) - \epsilon)\partial_y + \sin(2\pi z)\partial_x$, $\Lambda(z) = 2\pi\hat{s}z - \alpha\sin(2\pi z)$, $\tilde{J} = \nabla_\perp^2\tilde{\psi}$. The time ($t$), parallel ($z$) and perpendicular ($x, y$) normalization scales are $t_0 = (RL_n/2)^{1/2}/c_s$, $L_z = 2\pi q_a R$ and $L_0 = (\eta_{||}c^2L_z^2/(4\pi V_A^2 t_0))^{1/2}$, with an associated diffusion rate $D_0 = L_0^2/t_0$. The diamagnetic and MHD parameters are

$$\alpha_d = \frac{\rho_s c_s t_0}{(1+\tau)L_n L_0},\quad \alpha = q_a^2 R\frac{8\pi(p_{e0}+p_{i0})}{B^2 L_p}. \tag{4}$$

Unless noted otherwise, we consider the values $\hat{s} = 1$, $\tau = T_{i0}/T_{e0} = 1$, $\epsilon_n = 2L_n/R = 0.02$, $\epsilon = a/R = 0.2$, $q_a = 3$, $\eta_i = L_n/L_{T_i} = 1$, $\eta_e = 1$, $m_i/m_p = 2$.

3 L-H Transition and Density Limit

Fig. (2) shows the normalized, poloidally averaged ion energy flux $\Gamma_{p_i} \simeq -\langle\tilde{p}_i\tilde{\phi}_y\rangle$ versus α for various values of α_d. For small $\alpha_d < 0.5$ the transport increases strongly with increasing α, while for larger $\alpha_d \sim 1$, the transport at higher α is suppressed. This reversal reflects the fact that the turbulence in the small and large α_d cases is driven by different mechanisms with contrary dependences on electromagnetic effects.

In the small α_d case, the turbulence results mainly from the nonlinear development of resistive ballooning modes [9]. The enhancement of the transport at higher α in this case is due to the dependence of the turbulence saturation level on magnetic field perturbations, which strengthen as α is increased[4]. For very small $\alpha_d \lesssim 0.3$ the transport becomes extremely large even at small $\alpha \sim 0.3$. The evolution of the edge into this regime would lead to a large flux of plasma from the core into the edge and a possible radiation collapse. Since $\alpha_d \propto T/\sqrt{n}$ while $\alpha \propto nT$, the limit of small α_d and finite α is consistent with larger n and smaller T, and we label in Fig. (1) the rough boundary of this effectively forbidden zone as a "density limit". In agreement with this, evaluating α_d and α based on the edge discharge parameters at the density limit in AUG [10] ($R = 165cm$, $a = 50cm$, $B = 2.5T$, $T_e = 50ev$, $n \sim 3\times10^{13}/cm^3$, $Z_{eff} = 2$, $q = 4$), we obtain $\alpha_d \sim 0.3$, $\alpha \sim 0.5$. The energy diffusion rate predicted by the simulations for these parameters is immense: $D = \Gamma_{p_i}D_0$ with $D_0 \sim 60m^2/s$ and (see Fig. (2)) $\Gamma_{p_i} \sim 1$. This picture is also consistent with observations on Alcator-C that confinement degrades as the density limit is approached [3].

In the case $\alpha_d \sim 1$, resistive ballooning modes are weakened by diamagnetic effects [9], and the turbulence is predominantly caused by a nonlinear electron drift wave instability [9, 12, 11]. This instability relys on the nonlinear production of poloidal pressure gradients, which (unlike radial gradients) excite unstable drift waves even in the presence of the equilibrium magnetic shear[12]. The drift waves then grow due to the convection of the electron pressure across the magnetic field, which generates a parallel pressure gradient $\nabla_{||}p_e$ and an associated parallel current through Ohm's law [12]. This process, however, is inhibited by electromagnetic effects at very small α. This is because the electrons at higher α convect the magnetic field together with the electron pressure, leading to a large reduction of $\nabla_{||}p_e$ relative to the electrostatic, $\alpha = 0$ limit. This effect can be illustrated by a linear analysis of a constant ambient density gradient in the y-direction $n = n_0' y$ [6]. The resulting drift wave growth rate is strongly suppressed with increasing α, consistent with Fig. (2). A similar effect was also invoked in Ref. [13].

Returning to the issue of transport barrier formation, in a stable system an increased pressure gradient leads to increased turbulence and enhanced flux, which in turn acts to flatten the gradient. The gradient therefore evolves to a state in which the energy flux and the sources balance. A transport barrier can form spontaneously if the flux *decreases* with increasing gradient. In dimensional units the particle flux (comparable to Γ_{p_i}) can be written as $\Gamma = (D_0 n_0 / L_n)\,\Gamma_n(\alpha_d, \alpha, \epsilon_n, ...)$. The dependence on the gradient enters explicitly through the scale length L_n, which decreases as the profiles steepen, as well as implicitly through the L_n-dependence of D_0, α_d, α, etc. Excluding the variation of Γ_n, the flux has a strong positive power dependence $\Gamma \sim n_0'^2$. The dependence of Γ_n on n' must therefore reverse this for the system to be unstable to the formation of a barrier. This dependence, neglecting the weak variation of $\alpha_d \sim n'^{1/4}$, appears mainly through the parameters $\alpha \sim n'$ and $\epsilon_n \sim n'^{-1}$. For small α_d, Γ_n is insensitive to ϵ_n and increases sharply with α (see Fig. (2)), which reinforces the stability of the system. No barrier formation is therefore possible for small α_d.

At higher $\alpha_d \sim 1$, on the other hand, the α-dependence of Γ_{p_i} ($\sim \Gamma_n$) shown in Fig. (2) is reversed, allowing the possibility that $d\Gamma_n/d|n'|$ could change sign. The suppression associated with increasing α in this case must compete with the contrary n'^2 dependence of the normalization, as well as a strong destabilizing trend due to decreasing $\epsilon_n = 2L_n/R$ [9]. To determine the net dependence on the scale length, simulations were carried out in the range $\epsilon_n \sim 0.01 - 0.04$ for various values of α_d, α. After steady transport levels were established, the profile scale lengths were decreased and the parameters consistently adjusted. These simulations show $d\Gamma_n/d|n'|$ indeed changes sign, provided $\alpha \gtrsim 0.4$. The parametric boundary along which $d\Gamma_n/d|n'| = 0$ separates the L and H mode regimes in Fig. (1), and represents the L-H transition condition in our model. This prediction is supported by a study of Alcator C-Mod [14] and AUG [15] edge parameters at the L-H transition.

Poloidal $E \times B$ shear flows, generated locally by the turbulence, lead in part to the large transport reduction with increasing α_d seen in Fig. (2). The ordering on which our model is based, however, excludes a contribution to the E_r shear that can arise from profile variations beyond the intrinsic turbulence scale. This possibly understates the importance of E_r shear since such profile shear will reinforce the stability of the system during the steepening process [7, 8]. To address this issue, we carried out simulations of the edge pedestal in the context of a simple model. The model includes a source and sink (radially periodic) in the density equation (3), intended to represent neutral particle fueling in the edge. In response to the source, a modulation of the density profile develops that steepens the gradient in the center of the simulation domain. The strength of the source is chosen so that for $\alpha_d \sim 1$ and $\alpha \ll 1$ the source produces only a slight steepening of the profile before the system comes into equilibrium. We then slowly increase α with time. With increasing α the transport drops and the source causes the gradient to steepen, enhancing the turbulence until a new equilibrium is reached. At a critical value of α the region of maximum pressure gradient exceeds the L-H threshold condition and the profiles spontaneously begin to steepen. The subsequent evolution depends on the parameter ϵ_n: at $\epsilon_n = 0.02$ it is smooth and monotonic, while at $\epsilon_n = 0.01$ it is bursty. Fig. (3a) shows the flux $\Gamma_{p_i}(t)$ from a simulation that includes the source in the latter case, with $\alpha_d = 1$ and (initially) $\alpha = 0.05$. At $t = 1550$ the source is turned on and the value of α is slowly increased at a rate $d\alpha/dt = 2.5 \times 10^{-3}$. This causes the transport to drop gradually until $t = 1630$ ($\alpha \simeq 0.25$), when a burst of turbulence produces a large $E \times B$ poloidal sheared flow. This can be seen in Fig. (3b), which shows the time evolution of the root mean square poloidal $E \times B$ velocity $\bar{v}_{Ey} \equiv \langle \langle v_{Ey} \rangle_{y,z}^2 \rangle_x^{1/2}$ (dotted line), ion diamagnetic velocity $\bar{v}_{diy}$ (dashed), and total ion rotation $\bar{v}_{iy} = \overline{v_{Ey} + v_{diy}}$ (solid). This $E \times B$ flow sharply reduces the flux and induces a localized transport barrier (much smaller than the box size), which in turn leads to a steepening of the density profile that is reflected in a slow rise of the ion diamagnetic flow from 1650 to 1750. At $t = 1750$ ($\alpha \simeq 0.5$) the barrier is disrupted by a large scale resistive ballooning mode which again produces strong $E \times B$ sheared flow and suppression of the transport. A similar event at $t \simeq 1820$ leads finally to the formation of a global transport barrier at $t = 1920$. Beyond this, the diamagnetic velocity in Fig. (3b) increases monotonically as the profiles continue to steepen, while the total ion flow slowly decays due to effect of magnetic pumping. Since $v_{iy} = v_{Ey} + v_{diy} \simeq 0$, this forces $\bar{v}_{Ey}$ to increase in proportion to $\bar{v}_{diy}$, as seen in the figure. The growth of v_{Ey} reinforces the bifurcation of the system by suppressing turbulence in the pedestal everywhere except in a small region surrounding the maximum pressure gradient where $E_r' \simeq 0$.

4 Pedestal Stability

The steepening of the profiles following the transition in our simulations is not limited by the ideal $n \to \infty$ stability boundary. This is shown in Fig. (4), which is a plot of the ion pressure profile at an early time (dashed) and late time (solid, roughly $1000t_0$ after the transition) in a simulation with $\epsilon_n = 0.02$, $\alpha_d = 1$. The α-value at the center of the pedestal, $\alpha(x = 0) = 1.6$, is well beyond the first stability limit ($\alpha = 0.8$ at $\hat{s} = 1$). Shortly after the time of Fig. (4), however, the onset of a rapidly growing global mode with $k_y = 0.4$ (poloidal wavelength equal to the box-size) in the $E_r' \simeq 0$ region leads finally to a complete disruption of the pedestal. Further simulations show the onset of this mode occurs when $\alpha \simeq 1.6 \simeq 2\alpha_{crit}$ in the center of the pedestal, irrespective of the radially averaged value of α at the time of the crash. Global mode activity begins early in the simulation and appears at first in the form of two weakly growing modes. These modes propagate in both the ω_{*e} and ω_{*i} directions and closely resemble the two dominant linear resistive ballooning modes in our system at $k_y = 0.4$. One of these modes (the ω_{*i} root) eventually transitions to the rapidly growing instability that destroys the pedestal.

The clear violation of the ideal $n \to \infty$ stability limit in our simulations is consistent with MHD analyses of data from DIIID [16] and other tokamaks, which show the steep gradient region of an H-mode edge pedestal may well exceed the first ideal stability boundary. We offer here an explanation for this based on our analysis of a simple ramp-gradient model (discussed below). That analysis shows long wavelength ideal modes with $k_y < 1/L_p$ are stable because the radial localization of the pedestal gradient greatly weakens the drive of such modes relative to the stabilizing contribution of magnetic line-bending. Shorter wavelength modes with $k_y \gtrsim 1/L_p$, on the other hand, are stabilized by a combination of ω_{*i} and $E \times B$ shear effects.

To explore the behavior of ideal modes in the presence of a radially localized gradient, we consider a simple isothermal system in which the background density gradient (normally $n_0' = -1$ in our normalized units) is finite only in a localized region $-\delta < x < \delta$, and vanishes elsewhere ($n_0' = 0$). To be consistent with the pedestal simulations discussed above, we assume the equilibrium $E \times B$ and ion-diamagnetic flows balance: $\phi_0' = -\tau\alpha_d n_0'$. As a further simplification we eliminate the z-dependence of the configuration by taking $\hat{C} = -n_0' d/dy$ (i. e. bad curvature everywhere) and $\hat{s} = 0$, and in analogy to ballooning modes consider modes varying as $\exp(\gamma t + ik_y y + ik_z z)$ with $k_z = 2\pi$ fixed. Finally, we exclude resistive modes by dropping the resistive term (J term) in Ohm's law (1), and neglect the (small) terms proportional to ϵ_n. With these simplifications, Eqs. (1,2,3) may be combined to yield

$$\partial_x \left[(\gamma\gamma_* + 1/\alpha)\partial_x \tilde{f}(x)\right] = k_y^2(\gamma\gamma_* + 1/\alpha + n_0')\tilde{f}(x) \tag{5}$$

where $\gamma_* = \gamma + i\omega_{*i}$, $\omega_{*i} = -n_0' k_y \tau\alpha_d$, $\tilde{f} = \tilde{\phi}/\gamma_*$. The solution for $\tilde{f}(x)$ that is asymptotically well behaved at large x and continuous at $x = \pm\delta$ is given by $\tilde{f} = \exp(-k_y|x - \delta|)$ for $|x| > \delta$ ($n_0' = 0$), and $\tilde{f} = \cos(k_x x)/\cos(k_x\delta)$ for $|x| < \delta$ ($n_0' = -1$) (even solutions turn out to be the most unstable). Substituting this form into Eq. (5) for $|x| < \delta$ yields

$$\gamma\gamma_* = \frac{k_y^2}{k_y^2 + k_x^2} - \frac{1}{\alpha} \tag{6}$$

where k_x is determined by integrating Eq. (5) across $x = \pm\delta$ as

$$k_x \tan(k_x\delta) = k_y \left(\frac{\gamma^2 + 1/\alpha}{\gamma\gamma_* + 1/\alpha}\right) \ . \tag{7}$$

In the limit $k_y\delta \gg 1$, the k_x value of lowest order mode obtained from Eq. (7) is $k_x \approx \pi/(2\delta)$, and so Eq. (6) reduces in this limit to the local result $\gamma\gamma_* \simeq \gamma_0^2 = 1 - 1/\alpha$ with the usual stability condition $\omega_{*i}^2 > 4\gamma_0^2$. In the long wavelength limit, $k_y\delta \ll 1$, on the other hand, Eq. (7) reduces to $k_x^2 \simeq k_y/\delta$ (the right side of Eq. (7) approaches unity for $k_y \to 0$), and so Eq. (6) gives $\gamma^2 \simeq k_y\delta/(1 + k_y\delta) - 1/\alpha \simeq -1/\alpha$. That is, for $\alpha \sim 1$, ideal modes are always stable for $k_y \ll 1/\delta$, independent of ω_{*i}. This stabilization is due physically to the contribution of magnetic line-bending, which (unlike the ballooning drive term $\propto n_0'$) remains strong in the exterior region out to large distances $x \sim 1/k_y \gg \delta$.

We now turn to the case of arbitrary k_y and the numerical solution of Eqs. (6), (7). These equations depend only on the quantities $k_x\delta$, $k_y\delta$, γ, α, and the normalized ion-diamagnetic velocity

$$\hat{v}_{*i} = \frac{V_{*i}t_0}{\delta} = \frac{\rho_i}{\delta}\left(\frac{T_i}{T_i + T_e}\frac{R}{2L_p}\right)^{1/2} \qquad (L_p = p/|p'|). \tag{8}$$

Solving Eqs. (6), (7) numerically for fixed values of α, $\hat{v}_{*i}$, and maximizing the growth rate over all $k_y\delta$ yields a universal stability diagram shown in Fig. (5) (generalized to allow an arbitrary ideal MHD first stability threshold at $\alpha = \alpha_{crit}$). At late times in the pedestal simulation discussed earlier, the parameter $\hat{v}_{*i} \sim 1$. Similarly, evaluating $\hat{v}_{*i}$ in the H-mode pedestal based on recent data in DIIID [16] ($\delta \sim 6\rho_i \sim 0.0075R$) we obtain $\hat{v}_{*i} \sim 1$. For such $\hat{v}_{*i}$, Fig. (5) shows diamagnetic effects lead to an up-shift in the stability boundary of the pedestal (solid line) by more than a factor of two relative to the prediction of ideal $n \to \infty$ theory (dashed line). This explains why the local maximum value of α in the simulations, and possibly also the experiments [16], can exceed α_{crit}. Further, the steepening of the pedestal gradient following the transition in our simulations leads to a trajectory in the $\alpha - \hat{v}_{*i}$ space of Fig. (5) that eventually intersects the unstable region near $\alpha \sim 2\alpha_{crit}$. Thus, Fig. (5) is also consistent with the apparent onset of an ideal mode in the simulations at such a value of α.

5 Conclusion

We have argued the L-H transition and the density limit in tokamaks are fundamentally linked to the dependence of the turbulent edge transport on the parameters α and α_d as shown in Fig. (1). While the thresholds shown in the figure are likely to depend on important factors not discussed here, in particular T_i/T_e, non-circular geometry, and $\hat{s}$, we expect the framework on which they are based to be robust. We also find the steepening of the pedestal gradient following the L-H transition in our simulations can substantially exceed the stability limit predicted by ideal MHD for $n \to \infty$ ballooning modes. This breakdown of ideal MHD theory is due to the radially localized nature of the pedestal gradient, as well as the contribution of ion diamagnetic effects.

Acknowledgments

We acknowledge extensive discussions with Drs. T. Carlstrom, M. Greenwald, R. Groebner, A. Hubbard, R. Moyer, T. Osborne, W. Suttrop, and D. Thomas.

References

[1] F. Wagner, *et al.*, Phys. Rev. Lett. **49**, 1408 (1982)

[2] K. Burrell, *et al.*, Phys. Fluids **B2**, 1405 (1990).

[3] M. Greenw ald,*et al.*, Nucl. Fus. **28**, 2199 (1988)

[4] B. N. Rogers and J. F. Drake, Phys. Rev. Lett. **79**, 229 (1997).

[5] B. D. Scott, Plasma Phys. and Controlled Fusion **39**, 1635 (1997).

[6] B. N. Rogers, J. F. Drake, A. Zeiler, Phys. Rev. Lett. **81**, 4396 (1998).

[7] K. Burrell, *et al.*, in *Plasma Physics and Controlle d Nuclear F usion R ese ar ch*(IAEA, Vienna, 1994), V ol. I, p. 221.

[8] P . H. Diamond,*et al.*,*ibid*, paper D-2-II-6.

[9] A. Zeiler, *et al.*, Phys. Plasmas **3**, 2951 (1996).

[10] W. Suttrop, private communication.

[11] B. D. Scott, Plasma Phys. and Controlled Fusion **39**, 471 (1997).

[12] J. F. Drake *et al.* , Phys. Rev. Lett. **3**, 494 (1995).

[13] O. P ogutse, *et al.*, *24th Europ ean Physical So ciety Conferenc e on Controlle d F usion and Plasma Physics*, Berch tesgaden (European Physical Society, P etit-Lancy 1997), V ol.3, p. 1041

[14] A. Hubbard, *et al.*, Plasma Phys. and Controlled Fusion **40**, 689 (1998)

[15] "Operational Limits for High Edge Density H-Mode T ok amak Operation", W. Suttrop, *et al.*, J. of Nucl. Materials, in press (1998)

[16] R. J. Groebner and T. H. Osborne, Phys. Plasmas **5**, 1800, (1998)

FIGURES

FIG. 1. Edge plasma phase space

FIG. 2. , $_{p_i}(\alpha)$ for $\alpha_d = 0.25$ (square); $\alpha_d = 0.5$ (triangle); $\alpha_d = 0.75$ (ast); $\alpha_d = 1$ (diam)

FIG. 3. (a) , $_{p_i}$ vs. t at $\epsilon_n = 0.01$; (b) Ion drifts vs. t: $\bar{v}_{iy}$ (solid); $\bar{v}_{diy}$ (dash); $\bar{v}_{Ey}$ (dot)

FIG. 4. Early (dash), late (solid) ion pressure profiles.

FIG. 5. Stability boundary for ideal curvature driven modes

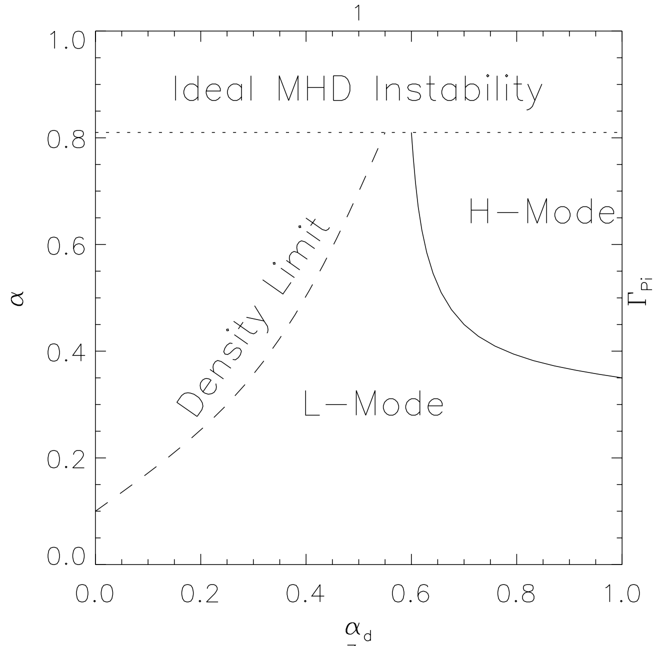
1
Ideal MHD Instability
H−Mode
Density Limit
L−Mode
α
α_d

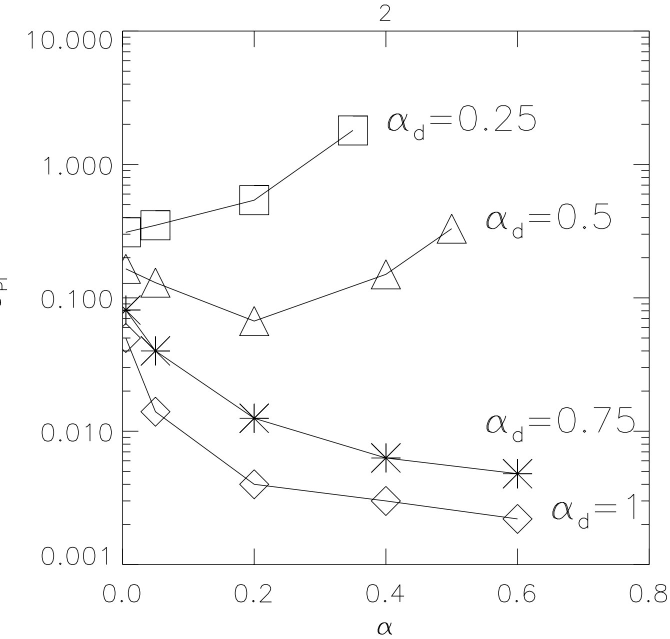
2
α_d=0.25
α_d=0.5
α_d=0.75
α_d=1
Γ_Pi
α

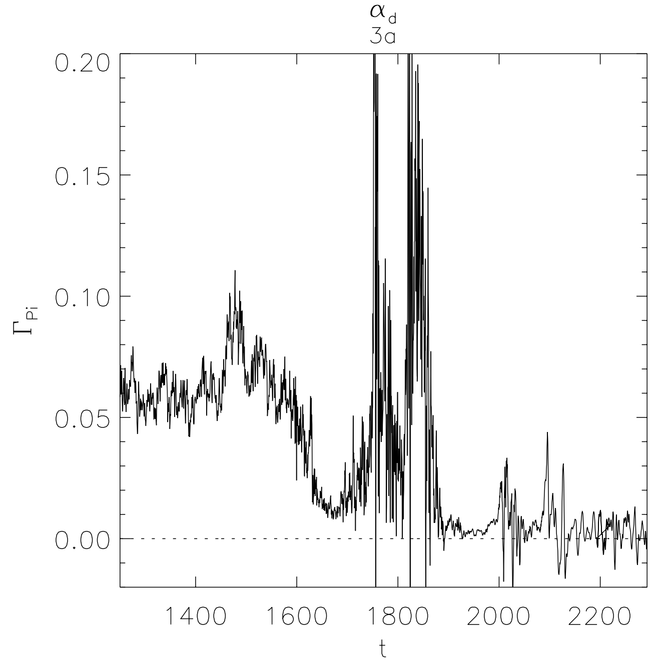
3a
Γ_Pi
t

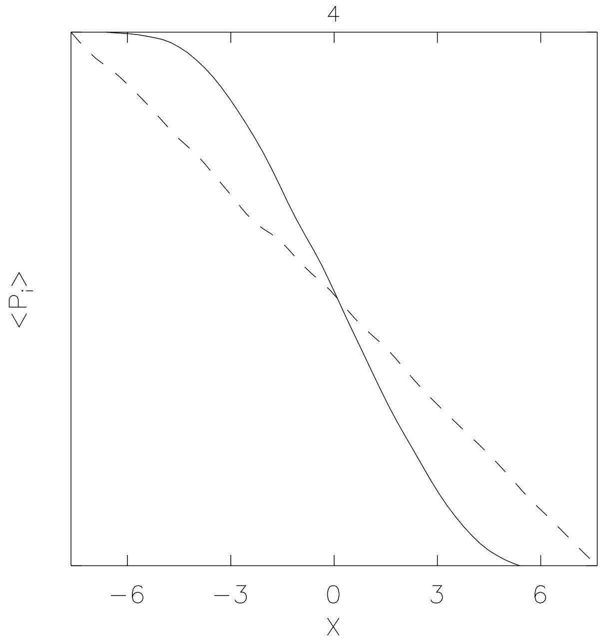
4
<P_i>
X

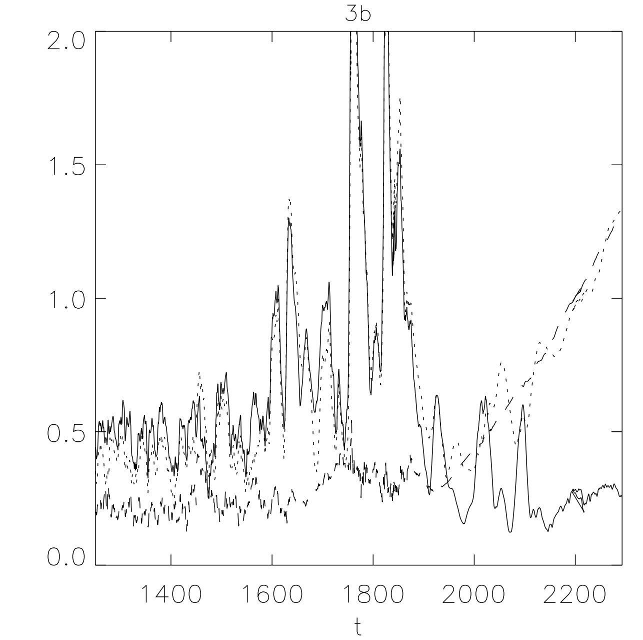
3b
t

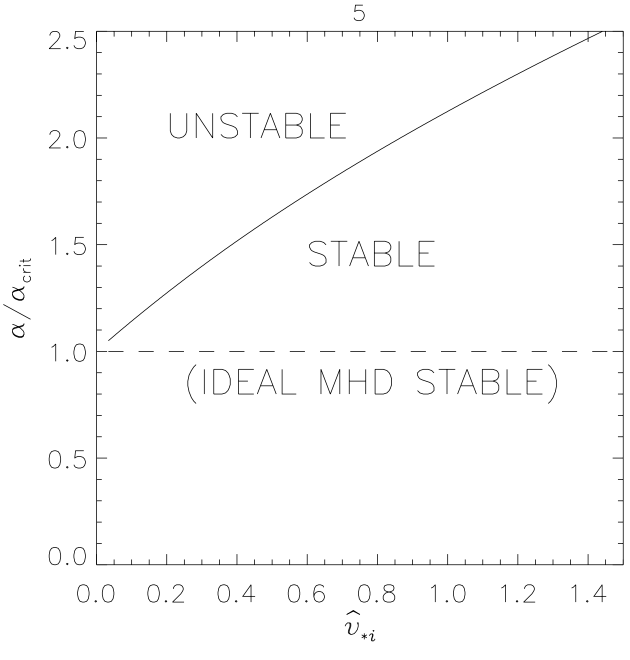
5
UNSTABLE
STABLE
(IDEAL MHD STABLE)
α/α_crit